HHS Public Access

Author manuscript

*Angew Chem Int Ed Engl*. Author manuscript; available in PMC 2021 March 16.

Published in final edited form as:

*Angew Chem Int Ed Engl*. 2020 March 16; 59(12): 4806–4813. doi:10.1002/anie.201916287.

# Polyhydrazide-based organic nanotubes as extremely efficient and highly selective artificial iodide channels

**Arundhati Roy**[+],
NanoBio Lab, 31 Biopolis Way, The Nanos, Singapore 138669 (Singapore)

**Himanshu Joshi**[+],
Department of Physics and Beckman Institute for Advanced Science and Technology, University of Illinois at Urbana-Champaign Urbana, Illinois, 61801 (USA)

**Ruijuan Ye**,
Department of Chemical and Biomolecular Engineering, National University of Singapore, Singapore 117585 (Singapore)

**Jie Shen**,
NanoBio Lab, 31 Biopolis Way, The Nanos, Singapore 138669 (Singapore)

**Feng Chen**,
NanoBio Lab, 31 Biopolis Way, The Nanos, Singapore 138669 (Singapore)

**Aleksei Aksimentiev**,
Department of Physics and Beckman Institute for Advanced Science and Technology, University of Illinois at Urbana-Champaign Urbana, Illinois, 61801 (USA)

**Huaqiang Zeng**
NanoBio Lab, 31 Biopolis Way, The Nanos, Singapore 138669 (Singapore)

## Abstract

We report herein a series of pore-containing polymeric nanotubes based on an H-bonded hydrazide backbone. Nanotubes of suitable lengths, possessing a hollow cavity of ~ 6.5 Å in diameter, are interestingly found to mediate highly efficient transport of diverse types of anions, rather than cations, across lipid membrane. Polymer channel **1a**, having an averaged molecular weight of 18.2 KDa and 3.6 nm in helical height, exhibits the highest anion transport activities with iodide ($EC_{50}$ = 0.042 μM or 0.028 mol% relative to lipid) being transported 10 times more efficiently than chlorides ($EC_{50}$ = 0.47 μM). Notably, even in cholesterol-rich environment, iodide transport activity still remains high with $EC_{50}$ of 0.37 μM. Molecular dynamics simulation studies confirm that the channel is highly selective for anions and that such anion selectivity arises from a positive electrostatic potential of the central lumen rendered by the interior-pointing methyl groups.

[+]These authors contributed equally to this work.

**Keywords**

Supramolecular chemistry; Anion channel; Iodide channel; Iodide deficiency disorders; MD simulation

## Introduction

Transport of anions is crucial for precise regulation of physiological processes.[1] As one of the essential elements of our body, iodides help to synthesize thyroid hormones, i.e., triiodothyronine and thyroxine.[2] They also help in proper bone development, *i.e.,* skeletal growth. The $Na^+/I^-$ symporter (NIS) is a transmembrane glycoprotein, which was identified to facilitate $I^-$ transport into the follicular cells of thyroid gland, a first step in thyroid hormone biosynthesis.[3] Since most of the thyroid cancer and breast cancer expresses NIS, radioactive $^{131}I$ has been routinely used for the imaging and treatment of these cancers. However, most of the times, they express insufficient NIS that triggers feeble uptake of $^{131}I$. Further, dysregulation of $I^-$ through NIS causes Iodide Deficiency Disorders (IDD)[4] on key organs such as brain, kidney, liver, heart and muscle.

Considerable interest has been invested in developing ion transport machinery for selective transport of chloride in lipid bilayer membranes [5] This is not only to understand the fundamental transport mechanism in biology but also for possible medical applications in channelopathies[6] or as anticancer agents.[5m,7] However, synthetic iodide channels are still underexplored, considering that only two iodide-selective channels have been reported thus far.[8] The first iodide channel reported by Gin is based on the $\beta$-cyclodextrin, exhibiting low activity and low selectivity among halides ($I^- > Br^- > Cl^-$).[8a] Recent work by Kim has shown that a porphyrin-based covalent organic cage can achieve high $I^-/Cl^-$ selectivity but with quite moderate iodide transport activity.[8b] As such, there is a need to develop highly active and selective artificial iodide transporters for potential medical treatment of IDD.

In 2004, Li reported a series of hydrazide-based aromatic foldamers that can fold via intramolecular H-bonds into well-defined cavity-containing curved conformations (for its general structure, see Figure 1), with the longest heptamer taking a one- turn helical structure.[9] Later on, the same group prepared short oligomers containing.5 to 11 building blocks as well as a short polymer sample having 20 building blocks and a helical height of 1.1 nm.[10] Exterior modification using triphenylalanine-based side chains enables these molecules to transport cations over anions in order of $NH_4^+ > Cs^+ > Rb^+ > K^+ > Na^+$.

Nevertheless, a large dimension of 9 Å x 11 Å (W x H, Figure S1) of the triphenylalanine side chains, which is not compatible with a typical aromatic $\pi$-$\pi$ stacking distance of 3.4 Å, might distort the central helical backbone and alter its intrinsic ion transport properties. This perspective prompted us to prepare longer polymers containing only straight alkyl chains arrayed around the exterior to examine the true ion-transporting properties.

Our motivation to prepare longer polymers is geared toward producing fully H-bonded, helically folded, cavity-containing nanotubes that can span the hydrophobic region of a lipid membrane (~ 3.4 nm, Figure 1). Achieving this through polymerization has proven to be a

challenging task,[11] which mostly can be ascribed to the low reactivity of amines and carboxylic acids that are destined to form covalent bonds highly rigidified by intramolecular H-bonds. In fact, despite availability of diverse types of fully H-bonded aromatic foldamers[12] since the pioneering works,[13] the hitherto reported longest nanotube with a fully H-bonded aromatic tubular cavity carries an average of 30 repeating units and a helical height of 1.4 nm,[11a,14]l while partially H-bonded polymers with a more flexible backbone could reach 6.1 nm.[11a]

In this work, we, for the first time, report successful production of fully H-bonded helically folded polymeric foldamers that possess a long tubular cavity of as much as 14 nm in height, via polymerization of two readily accessible repeating units **A** and **B** (Figure 1). Importantly, our above surmise turns out to work out perfectly well, although in a somewhat surprising fashion. That is, in sharp contrast to preferred transport of cations over anions as reported by Li,[10] we demonstrate that alkyl chain-appended polymers of 2.1 – 5.4 nm in helical height and ~ 6.5 Å in cavity diameter (Figure 1c) promote a highly selective transport of anions, rather than cations, across lipid membrane.

## Results and Discussion

### Synthesis of long polymers of 2.1 – 5.4 nm in helical height.

Early attempts to prepare fully H-bonded polymeric aromatic foldamers often used the acyl chloride coupling method.[10] [11a] Following this method to test a few polymerization conditions for coupling **A** and **B**, we found that 6.7 KDa (about 3.9 helical turns and 1.3 nm in helical height) is about the highest molecular weight we can obtain (entry 18 of Table S1). This is consistent with 1.1 nm in height obtained by Li for the same type of polymers with different side chains.[10]

Encouraged by our recent findings that amide coupling reagent BOP could mediate efficient formation of sterically hindered H-bond-rigidified amide bonds,[15] we decided to scrutinize the polymerization efficacy of 17 amide coupling agents. For convenience of recording, polymers with exterior side chains are classified as **1** (R = *n*-$C_8H_{17}$), **2** (R = *n*-$C_{12}H_{25}$) and **3** (R = *n*-$(CH_2CH_2O)_3CH_3$), while letters **a-r** designate one of the 18 coupling methods (17 coupling agents + acyl chloride) used to produce the polymer samples (Figure 2b and Table S1). For instance, polymer **1a** refers to a polymer sample with *n*-C8H17 as side chains and HATU as the coupling agent.

Units **A** containing three types of side chains were made from resorcinol by following a three-step protocol and further reaction with hydrazine hydrate.[16] The optimized polymerization conditions involve mixing A, B and coupling agent at a molar ratio of 1:1:3 in 6 mL of freshly distilled $CH_2Cl_2$/DMF (5:1, v:v) at room temperature, followed by addition of 100 μL DIEA (N,N- diisopropylethylamine). The polymerization reaction was allowed to take place for 2 days, with typical yields of 60 – 80 % for a total of 53 polymer samples (e.g., **1a-1r** except for **1h**, **2a-2r** and **3a-3r**). Their average molecular weights were determined by Gel Permeation Chromatography and listed in Table S1. Polymers **1a**, **1c**, **2a**, **2c** and **3c** displayed characteristic mass pattern of repeating unit in the MALDI spectra (Figure S2-S6).

## Efficient ion transport by polymer channels.

We evaluated the ability of these polymers to plug into lipid membrane and to transport ions across membrane using fluorescence assay (Figure 2a), which employs a pH-sensitive fluorescent dye HPTS (8-hydroxy-1,3,6-pyrenetrisulfonate) trapped inside egg yolk phosphatidylcholine (EYPC)-based large unilamellar vesicles (LUVs).[5a],[17] In this assay, a pH gradient of 7 to 8 was applied across the vesicles, and ion transport activities were monitored by increment of HPTS fluorescence ($\lambda_{ex}$ = 450 nm, $\lambda_{em}$ = 510 nm) over 300 s with that induced by Triton X-100 (added at $t$ = 300 s) set as 100% (Figure 2b).

Application of this pH-sensitive HPTS assay onto 17 polymer samples with $n$-$C_8H_{17}$ side chains (**1a-1g** and **1i-1r**, Figure 2b) reveals **1a**, having an average MW of 18.2 KDa and a height of 3.6 nm,[5c] exhibits the highest fractional transport activity of 102% at 1 μM. This high activity was followed by **1k** (100%), **1m** (97%), **1d** (77%), **1c** (73%) and **1b** (68%), with MWs of 10.8 – 27.3 KDa and heights of 2.1 – 5.4 nm. The remaining 11 samples, with low fractional activities of < 25%, are characterized by low (< 10 KDa) or high (> 30 KDa) molecular weights. These results are largely consistent with hydrophobic membrane thickness of 3.4 nm.

As summarized in Figures 2c, S12 and S13, using the same HPTS assay at the same concentration (1 μM), the best channels for series **2** and **3** are **2h** (15%, MW = 33 KDa) and **3d** (37%, MW = 3.4 KDa), respectively. Generally, these are results of poor solubility of **2** and too good solubility of **3** in buffer at **1** μM. Overall, polymer channels **1** display much better activities than **2** and **3**, likely due to their more favoured lipophilic character that leads to more efficient channel incorporation into lipid membrane. **1a**, the most active channel among 53 polymer channels, was assessed in a dose-dependent manner for Hill Analysis (Figures 2d and S14). The calculated $EC_{50}$ value of 0.47 μM (0.31 mol% relative to lipid) indicates an excellent ion transport activity by **1a**.

## Preferential transport of anions over cations.

For the HPTS assay used for assaying ion transport activities, increment of fluorescence could be due to ion exchange through antiport ($H^+/Na^+$ and $Cl^-/OH^-$) or symport ($H^+/Cl^-$ and $Na^+/OH^-$) mechanisms. To discern these mechanisms, three sets of assays were performed (Figure 2e-g). At first, both $H^+$ and $Na^+$ transports were evaluated using LUVs containing HEPES (10 mM) and $Na_2SO_4$ (100 mM) at pH = 7.0, which were dispersed in the same buffer (10 mM HEPES, 100 mM $Na_2SO_4$) at pH = 8.0. Channel **1a** at 1 μM was found to be non-responsive towards transport of $H^+$ or $Na^+$. In contrast, both ion transporter gramicidin A (gA) at 2 μM and proton transporter FCCP (carbonyl cyanide 4-(trifluoro methoxy)phenylhydrazone) at 1 μM result in substantial transport activity (Figure 2e). These results rule out both $H^+/Na^+$ antiport and $Na^+/OH^-$ symport as the likely mechanisms. Similarly, both variation of extravesicular metal ions ($M^+$ = $Li^+$, $K^+$ and $Cs^+$, Figure 2e), and the assay with very high salt gradient (200 mM $Na_2SO_4/K_2SO_4$, Figure S15) reveal very low transport of cation, confirming that it is anions, not cations, that mainly participate in the ion transport process.

Next, SPQ (6-Methoxy-*N*-(3-Sulfopropyl)Quinolinium) whose fluorescence intensity decreases in the presence of increasing concentrations of $Cl^-$ was introduced into extravesicular region of LUVs (Figure 2f).[18] The observed concentration-dependant quenching of SPQ for channel **1a** at 0.2 – 1.0 μM provides direct proof of **1a**-mediated chloride influx into LUV.

To additionally differentiate the transport rates between $Cl^-$ and $OH^-$ or $H^+$, proton transporter FCCP was applied in the HPTS assay (Figure 2g).[18] That transport activities of **1a** (0.5 μM) were found to be comparable in presence (49%) or absence (50%) of FCCP suggests $H^+$ or $OH^-$ transport rates to be faster than that of $Cl^-$, which constitutes the rate limiting step. Further, MD results clearly point to the formation of the water chains (Supporting movie SM3), and these water chains should facilitate rapid transport of $H^+$, not $OH^-$, via the Grotthuss mechanism across membrane in order to maintain the charge balance.

## Membrane integrity in the presence of polymer channels.

Membrane integrity in the presence of channel molecules was then established by carboxyfluorescein-leakage assay ($\lambda_{ex}$ = 492 nm, $\lambda_{em}$ = 517 nm, Figure S16). Specifically, addition of **1a** at 1 μM causes only 4% increase in carboxyfluorescein fluorescence, while Melittin, which induces membrane lysis, results in 56% and 91% increases at 0.15 and 0.2 μM, respectively. These comparative data demonstrate that **1a** does not lysate the membrane and possesses a pore size of < 1 nm across.

To exclude other possible membrane defects (spaces between bundles of polymer tubes, interface between the gel and fluid phases of lipids surrounding the polymer tubes, etc) that may be responsible for the observed anion transport, **1a** was modified at its two ends using a sterically bulky benzyl group (W × L = 6.7 × 8.3 Å) to generate polymer **1a-Bn** (Scheme S2). Modification of **1a** with a monobenzyl group should not exert significant changes in its helical conformation since the strong intramolecular H-bonds will only direct these benzyl groups to point toward the channel's interior, rather than exterior. Thus, it is expected that **1a-Bn** differs insignificantly from **1a** in terms of association with the membrane lipids, and any possible membrane defects formed by **1a** should also persist for **1a-Bn**. Differing from **1a**, the inward-pointing benzyl groups in **1a-Bn** should at least partially block the channel cavity of 6.5 Å, resulting in either a reduction or complete loss in anion transport activity. Experimentally, **1a-Bn** indeed becomes incapable of transporting any anions (Figure S17), thereby supporting the notion that anion transport was mediated by the pore contained in **1a**, rather than membrane defects.

## Chloride transport by a channel mechanism and $Cl^-/K^+$ selectivity.

The ability of **1a** to transport anions via a channel mechanism was unambiguously confirmed by the observed single channel current traces for chloride transport, recorded in a planar lipid bilayer at various voltages in symmetric baths (*cis* chamber = *trans* chamber = 1 M KCl, Figure 3a). Linear fitting of current- voltage (I-V) plot gives rise to a $Cl^-$ conductance value ($\gamma_{Cl}$) of 1.19 ± 0.024 pS for **1a** (Figure 3a), with $Cl^-/K^+$ selectivity of 13 (Figures 3b and S18).

### High selectivity and high efficiency in iodide transport.

Using the HPTS assay illustrated in Figure 2h, selectivity in **1a**-mediated anion transport was investigated by replacing intravesicular NaCI with NaX ($X^- = Br^-$, $I^-$, $NO_3^-$ and $ClO_4^-$). From the determined $EC_{50}$ values obtained after correcting background signals (Figures 2h and S19), a selectivity topology, $I^- > ClO_4^- > NO_3^- > Br^- > Cl^- > SO_4^{2-}$, was obtained with $I^-$ ($EC_{50}$ = 0.042 μM, or 0.028 mol% relative to lipid) being transported 8 and 10 times faster than $Br^-$ ($EC_{50}$ = 0.38 μM) and $Cl^-$ ($EC_{50}$ = 0.47 μM), respectively. And both $ClO_4^-$ ($EC_{50}$ = 0.057 μM) and $NO_3^-$ ($EC_{50}$ = 0.08 μM) are also preferred transport species for **1a**. From these $EC_{50}$ values, transport selectivity of $I^-/K^+$ is estimated to be greater than 145. Significantly, in LUVs containing 33% cholesterol that is known to decrease membrane fluidity prominently, **1a** still functions well, with $EC_{50}$ values of 0.37 and 0.45 μM for $I^-$ and $ClO_4^-$ (Figures S20–S21), respectively.

To compare with Kim's highly selective iodide channel based on a porphyrin-derived covalent organic cage,[8b] the same assay condition by Kim was applied to **1a** (Figure S22). The resulting quenching of HPTS fluorescence follows the same selectivity sequence as reported. Remarkably, **1a**-mediated iodide influx results in 100% quenching at **[1a]** = 0.15 μM, with mere 14% and 8% for $Br^-$ and $Cl^-$, respectively. On the basis of initial rate constants (Figure S22), $I^-/CI^-$ selectivity was determined to be 42. Compared to **1a**, Kim's organic cage is more selective by 30% ($I^-/CI^-$ = 60), but its iodide transport activity is at least 17 times less active ($EC_{50}$ value > 0.5 mol%).

Lastly, to eliminate possible quenching effects the heavy iodine atom might have on the fluorescence intensity of the HPTS day, we have carried out titration experiments in the presence of iodide anions at concentrations ranging from 10 to 140 mM at pHs 7 and 8 (Figure S23). We found that at either pHs 7 or 8, a change in iodide concentation from 10 to 140 mM produces no more than 2% difference in fluorescence intensity of HPTS dye when compared to that at 100 mM. These data confirm that anions such as iodides exert insignfiicant influence on the HPTS dye. ln contrast, changes in pH from 7 to 7.5 or from 7 to 8 result in dramatic increases by 96% and 195% in fluorescence intensity of HPTS dye, respectively, demonstrating that HPTS dye is indeed far more sensitive to changes in pH than those in iodide concentration and that our observed iodide transport is not a result of fluorescence quenching by iodide anions.

### Computational insights into preferential transport of anions over cations.

To elucidate the microscopic mechanism of ion permeation through the polymeric channels, we built an all-atom model of the **HP24** channel containing 24 **A** and 24 **B** units and a height of 2.8 nm using psfgen plugin of VMD[19] (Figure S8a and Supporting Movies SM1 and SM2). The model was embedded in a patch of 1-palmitoyl-2-oleoyl-sn-glycero-3-phosphatidyl choline (POPC) membrane, which has a hydrophobic thickness of 2.8 nm. To characterize the structural dynamics and ion selectivity **of HP24**, we created several systems by solvating the membrane-embedded **HP24** channel with aqueous solutions of KCl, Kl, NaCl and Nal at 0.6 or 1 M. Figure S8b shows a typical configuration of a fully assembled all-atom simulation system.

First, we performed equilibrium MD simulations of the systems using a previously described simulation protocol.[20,21] Briefly, the channel was initially restrained allowing lipid molecules to equilibrate around the channel. After 100 ns, the channel was released, and the system was simulated free of any restraints for 550 ns. During this unrestrained equilibration, the channel maintained its initial structure, with local structural fluctuations stabilizing at about 3.5 Å root mean squared deviation value (Figure S8c). As soon as the simulation began, water molecules were observed to permeate through the interior cavity of the channel, from one side of the membrane to the other (Supporting Movie SM2). Within the 550 ns equilibrium of the 0.6 M NaCl system, we observed five $Cl^-$ ions entering and passing the channel, without observing $Na^+$ transport.

We computationally assessed the ability of the **HP24** channel to conduct ions by simulating the channel solvated in 1 M solution of KCl, Kl, NaCl or Nal under ±1V transmembrane voltage. Figure 4a shows a typical simulation system. Figure 4b plots the total charge transported through the channel as a function of simulation time for the KCl and Kl systems; Figure S9 shows similar data for the NaCl and Nal systems. The slope of the charge-versus-time trace yields the average currents for all simulated systems (Table S3). ln all the cases studied, the current was predominately carried by anions ($Cl^-$ and $l^-$), which contributed from 78 to 93% of the total current (Figures 4c and S9). While these simulations undoubtedly demonstrate the ability of **HP24** to conduct ions in an anion-selective manner, direct comparison of the simulated currents with experiment is not possible.[22] Further, the channel was observed to conduct more current under the negative transmembrane bias than under the positive bias. This rectification of ionic current can be explained by the presence of the negatively ($COO^-$) and positively ($NH_3^+$) charged group at the either entrance of the channel (Figure 4a).

To determine the near-equilibrium energetics of ion transport through **HP24** channel and its dependence on ion species, we have performed replica exchange umbrella sampling MD simulations.[23] The simulation system was divided into 69 windows using 1 Å bins arranged along the Z axis (the axis normal to the lipid bilayer plane). An ion was confined to remain within the respective windows using a harmonic potential (Figure 5a). The starting configuration for each window was obtained from a brief (1.4 ns) steered molecular dynamics (SMD) run. All 69 simulations were run in parallel for ~100 ns using the replica exchange umbrella sampling protocol.[24] Figure 5b shows the resulting potential of mean force (PMF) of $Cl^-$, $K^+$, and $l^-$ ions with respect to its Z coordinate. $K^+$ ion PMF is characterized by a single barrier in the middle of the membrane. The PMFs of $Cl^-$ and $l^-$ ions are qualitatively different: after initial increase, the PMF is largely flat in the middle of the channel, with some variations among the plateau that we attribute to local deformation of the channel's structures, in particular small fenestration at Z = 10 Å. With regard to the barrier amplitude, $K^+$ experiences the largest energy penalty, with the $l^-$ ions being smallest Thus, consistent with our experimental results, the PMF profiles clearly support both anion selectivity relative to cation and $l^-$ selectivity with respect to the $Cl^-$ ion. The presence of the periodic fine structure in the PMF of the $I^-$ ion ($-15 < Z < 0$) suggests a pronounced effect of the channel's chemical structure on the energetics of $I^-$ conductance. Figure S10a shows similar data for NaCI system, i.e., the $Cl^-$ ions are transported preferentially over $Na^+$ ions.

To determine the molecular mechanism of the ion selectivity, we examined hydration of ions in bulk solutions and when passing through the channel. First, we defined the solvation shell of each ion type from the water-ion radial distribution functions[25] (Figure S11). Figure 5c plots the average number of water molecules in the first solvation shell of the respective ion with respect to the ion's Z coordinate. Owing to its largest ionic radius, the $I^-$ ion possesses the largest solvation shell in the bulk followed by the $Cl^-$ and $K^+$ ions The solvation shell of the $I^-$ ions, however, loses the greatest number of water molecules as it enters in the channel. In fact, there are fewer water molecules surrounding $I^-$ ion in the channel than those surrounding the $Cl^-$ ion. This result, however, does not explain anion selectivity of the channel. By analyzing equilibrium MD trajectories,[26] we obtained the electrostatic potential map of the system (Figure 5d). The average electrostatic potential inside the central lumen of the channel is positive as compared to the bulk solution (Figure 5e), making the channel selective for anion transport. Finally, it has been suggested that the rate of transport through a channel is conditioned by the number of hydrogen bonds that the solute makes with the channel.[27] To see if this applies also to transport of solvated ions, we computed the average number of hydrogen bonds formed between the water molecules in the first solvation shell of the ion and the remaining part of the system (e.g., channel's interior functional groups as well as other water molecules not from the first solvation shell, Figure 5f). We found that the solvation shell of $I^-$ ion forms lesser number of hydrogen bonds as compared to $Cl^-$ ions, thereby giving rise to a more frictionless, faster transport of the $I^-$ ions.

Overall, the analysis of the simulations trajectories confirms that the channel is highly selective for anions, with the energetic barriers less for anions than those for cations. These reduced energy penalties in anion transport arise from a positive electrostatic potential of the central lumen rendered by the many methyl groups (from methoxy groups) that decorate the lumen. Corroborated by ionic current measurements in the applied electric field simulations and with the smallest energy barrier for I- relative to others (e.g., $Na^+$, $K^+$ and $Cl^-$) as seen from the free energy calculations using enhanced sampling method, it is evident that the **HP24** channel is most favorable for the transport of $I^-$ ions. And a fewer number of the hydrogen bonds formed by the water molecules in the first solvation shell of the $I^-$ ion provides the molecular basis that accounts for its faster more frictionless transmembrane transport than the $Cl^-$ ion.

## Conclusion

In summary, we have for the first time achieved efficient one-pot preparation of fully H-bonded helically folded aromatic foldamer-based nanotubes of 6.5 Å across and up to 14 nm in helical height, through the use of simple amide coupling agents such as HATU. These nanotubes carry an extensive array of oxygen atoms along their interior surface but are found to preferentially transport anions rather than cations. Moreover, lipophilicity and proper length was found to be crucial, with the most active polymer channel 1a carrying shorter octyl side chains and having a helical height of 3.6 nm. This polymer-based channel (1) displays an intrinsic excellent selectivity towards anions over cations, (2) prefers iodide over other inorganic anions with iodide being transported > 10 times better than chloride and (3) functions well in cholesterol-rich environment. Anion selectivity was confirmed and origin

of such selectivity was elucidated by all atom MD simulation studies. Given a high modularity in repeating units, a broad variety of polyhydrazide-based nanotubes, which possess a hollow cavity of wide-ranging diameters, can be readily envisioned for interesting applications.

## Supplementary Material

Refer to Web version on PubMed Central for supplementary material.

## Acknowledgements

This work was supported by the Institute of Bioengineering and Nanotechnology (Biomedical Research Council, Agency for Science, Technology and Research, Singapore), the Singapore National Research Foundation under its Environment and Water Research Programme and administered by PUB, the National Science Foundation (USA) under grant DMR-1827346 and the National Institutes of Health under grant P41-GM104601. Supercomputer time was provided through the Early Allocation grant on Frontera (FTA-Chemla), XSEDE Allocation Grant no. MCA05S028 and the Blue Waters petascale supercomputer system at the University of Illinois at Urbana-Champaign.

## References

[1]. Duran C, Thompson CH, Xiao Q, Hartzell HC, Ann. Rev. Physiol. 2010, 72, 95–121. [PubMed: 19827947]

[2]. a) Ahad F, Ganie SA, Indian J. Endocrinol. Metabol. 2010, 14, 13–17;b) Chung HR, Ann. Pediatr. Endocrinol. Metabol. 2014, 19, 8–12.

[3]. Darrouzet E, Lindenthal S, Marcellin D, Pellequer J-L, Pourcher T, Biochim. Biophys. Acta Biomembr. 2014, 1838, 244–253.

[4]. Mina A, Favaloro EJ, Koutts J, Laboratory Medicine 2011, 42, 744–746.

[5]. a) Sidorov V, Kotch FW, Abdrakhmanova G, Mizani R, Fettinger JC, Davis JT, J. Am. Chem. Soc. 2002, 124, 2267–2278; [PubMed: 11878981] b) Schlesinger PH, Ferdani R, Liu J, Pajewska J, Pajewski R, Saito M, Shabany H, Gokel GW, J. Am. Chem. Soc. 2002, 124, 1848–1849; [PubMed: 11866586] c) Gorteau V, Bollot G, Mareda J, Perez-Velasco A, Matile S, J. Am. Chem. Soc. 2006, 128, 14788–14789; [PubMed: 17105272] d) Gorteau V, Bollot G, Mareda J, Matile S, Org. Biomol. Chem. 2007, 5, 3000–3012; [PubMed: 17728867] e) Li X, Shen B, Yao X-Q, Yang D, J. Am. Chem. Soc. 2009, 131, 13676–13680; [PubMed: 19772362] f) Yamnitz CR, Negin S, Carasel IA, Winter RK, Gokel GW, Chem. Commun. 2010, 46, 2838–2840;g) Vargas Jentzsch A, Matile S, J. Am. Chem. Soc. 2013, 135, 5302–5303; [PubMed: 23517007] h) Saha T, Dasari S, Tewari D, Prathap A, Sureshan KM, Bera AK, Mukherjee A, Talukdar P, J. Am. Chem. Soc. 2014, 136, 14128–14135; [PubMed: 25203165] i) Saha T, Gautam A, Mukherjee A, Lahiri M, Talukdar P, J. Am. Chem. Soc. 2016, 138, 16443–16451; [PubMed: 27933857] j) Wei X, Zhang G, Shen Y, Zhong Y, Liu R, Yang N, Al- mkhaizim FY, Kline MA, He L, Li M, Lu Z-L, Shao Z, Gong B, J. Am. Chem. Soc. 2016, 138, 2749–2754; [PubMed: 26877246] k) Shinde SV, Talukdar P, Angew. Chem. Int. Ed. 2017, 56, 4238–4242;l) Behera H, Madhavan N, J. Am. Chem. Soc. 2017, 139, 12919–12922; [PubMed: 28874045] m) Ren C, Ding X, Roy A, Shen J, Zhou S, Chen F, Yau Li SF, Ren H, Yang YY, Zeng HQ, Chem. Sci. 2018, 9, 4044–4051. [PubMed: 29780533]

[6]. a) Davis JT, Okunola O, Quesada R, Chem. Soc. Rev. 2010, 39, 3843–3862; [PubMed: 20820462] b) Brotherhood PR, Davis AP, Chem. Soc. Rev. 2010, 39, 3633–3647; [PubMed: 20714471] c) Matile S, Vargas Jentzsch A, Montenegro J, Fin A, Chem. Soc. Rev. 2011, 40, 2453–2474; [PubMed: 21390363] d) Kim DS, Sessler JL, Chem. Soc. Rev. 2015, 44, 532–546. [PubMed: 24984014]

[7]. a) Wu X, Judd LW, Howe Ethan N. W., Withecombe AM, Soto-Cerrato V, Li H, Busschaert N, Valkenier H, Perez-Tomas R, Sheppard DN, Jiang Y-B, Davis AP, Gale PA, Chem 2016, 1, 127–146;b) Ko S-K, Kim SK, Share A, Lynch VM, Park J, Namkung W, Van Rossom W, Busschaert N, Gale PA, Sessler JL, Shin I, Nat. Chem. 2014, 6, 885; [PubMed: 25242483] c) Smith BA,

Daschbach MM, Gammon ST, Xiao S, Chapman SE, Hudson C, Suckow M, Piwnica-Worms D, Gokel GW, Leevy WM, Chem. Commun. 2011, 47, 7977–7979.

[8]. a) Madhavan N, Robert Erin C, Gin Mary S, Angew. Chem. Int. Ed. 2005, 44, 7584–7587;b) Benke BP, Aich P, Kim Y, Kim KL, Rohman MR, Hong S, Hwang I-C, Lee EH, Roh JH, Kim K, J. Am. Chem. Soc. 2017, 139, 7432–7435. [PubMed: 28538099]

[9]. Hou J-L, Shao X-B, Chen G-J, Zhou Y-X, Jiang X-K, Li Z-T, J. Am. Chem. Soc. 2004, 126, 12386–12394. [PubMed: 15453772]

[10]. Xin P, Zhu P, Su P, Hou J-L, Li Z-T, J. Am. Chem. Soc. 2014, 136, 13078–13081. [PubMed: 25188764]

[11]. a) Zhang D-W, Wang H, Li Z-T, Macromol. Rapid Commun. 2017, 38, 1700179;b) Chen J-Y, Hou J-L, Org. Chem. Front. 2018, 5, 1728–1736;c) Chen F, Shen J, Li N, Roy A, Ye RJ, Ren CL, Zeng HQ, Angew. Chem. Int. Ed. 2019, 58, DOI: 10.1002/anie.201906341.

[12]. Zhang D-W, Zhao X, Hou J-L, Li Z-T, Chem. Rev. 2012, 112, 5271–5316. [PubMed: 22871167]

[13]. a) Hamuro Y, Geib SJ, Hamilton AD, Angew. Chem., Int. Ed. 1994, 33, 446;b) Zhu J, Parra RD, Zeng HQ, Skrzypczak-Jankun E, Zeng XC, Gong B, J. Am. Chem. Soc. 2000, 122, 4219–4220;c) Berl V, Huc I, Khoury RG, Krische MJ, Lehn JM, Nature 2000, 407, 720–723. [PubMed: 11048713]

[14]. van Gorp JJ, Vekemans JAJM, Meijer EW, Chem. Commun. 2004, 60–61.

[15]. a) BOP = ((Benzotriazol-1-yloxy)tris(dimethylamino)phosphoniumhexa fluorophosphate);b) Du ZY, Ren CL, Ye RJ, Shen J, Lu YJ, Wang J, Zeng HQ, Chem. Commun. 2011, 47, 12488–12490.

[16]. Zeng HQ, Miller RS, Flowers RA, Gong B, J. Am. Chem. Soc. 2000, 122, 2635–2644.

[17]. Ren C, Shen J, Zeng HQ, J. Am. Chem. Soc. 2017, 139, 12338–12341. [PubMed: 28837325]

[18]. Ren CL, Zeng F, Shen J, Chen F, Roy A, Zhou S, Ren H, Zeng HQ, J. Am. Chem. Soc. 2018, 140 8817–8826. [PubMed: 29927580]

[19]. Humphrey W, Dalke A, Schulten K, J. Mol. Graph. 1996, 14, 33–38. [PubMed: 8744570]

[20]. Gopfrich K, Li C-Y, Mames I, Bhamidimarri SP, Ricci M, Yoo J, Mames A, Ohmann A, Winterhalter M, Stulz E, Aksimentiev A, Keyser UF, Nano Lett. 2016, 16, 4665–4669. [PubMed: 27324157]

[21]. Decker K, Page M, Boyd A, MacAllister I, Ginsberg M, Aksimentiev A, ACS Biomater. Sci. Eng. 2017, 3, 342–348.

[22]. There are several reasons that could explain the difference between simulated and measured currents. (1) The applied potential is typically concentrated to the transmembrane region, with limited effect on ion entrance. That is, the high bias might wash out some barriers in the middle of the channel, without affecting the barriers at the channel entrance. This may explain why rectification is more pronounced at 1V. (2) With regard to rectification, it is also possible that the terminal groups in experiment do not maintain the same conformation as in simulations. Such partial unwinding is more likely on the experimental time scale. Without the charged group present right at the entrance of the channel, the rectification phenomenon should not happen. (3) There are potential inaccuracies regarding the channel structure and parameterization.

[23]. Sugita Y, Kitao A, Okamoto Y, J. Chem. Phys. 2000, 113, 6042–6051.

[24]. Roux B, Comput. Phys. Commun. 1995, 91, 275–282.

[25]. Rowley CN, Roux B. t., J. Chem. Theory and Comput. 2012, 8, 3526–3535. [PubMed: 26593000]

[26]. Aksimentiev A, Schulten K, Biophys. J. 2005, 88, 3745–3761. [PubMed: 15764651]

[27]. Horner A, Zocher F, Preiner J, Ollinger N, Siligan C, Akimov SA, Pohl P, Sci. Adv. 2015, 1, e1400083.

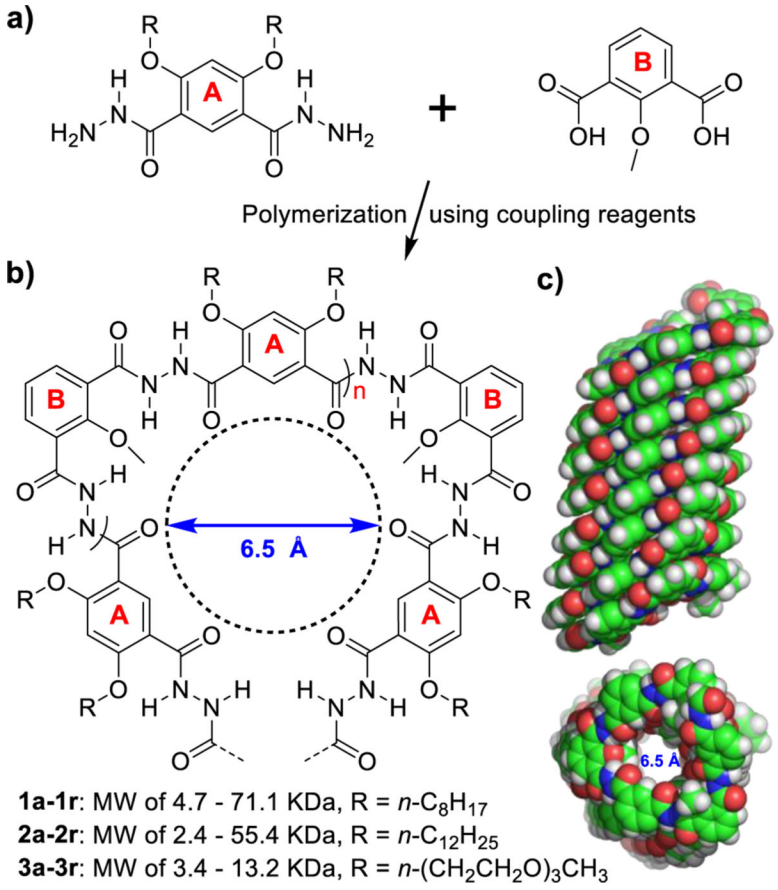


**Figure 1.**

a) Structures of building blocks **A** and **B** used to produce nanotubes **1–3**. b) Foldamer-based approach for constructing H-bonded pore-forming polymeric anion channels **1–3**, having a hollow cavity of 6.5 Å in diameter after excluding van der Waals volume of atoms decorating channel's interior. c) Side and top views of a helically folded polymeric nanotube computationally optimized in POPC membrane (Supporting Information).

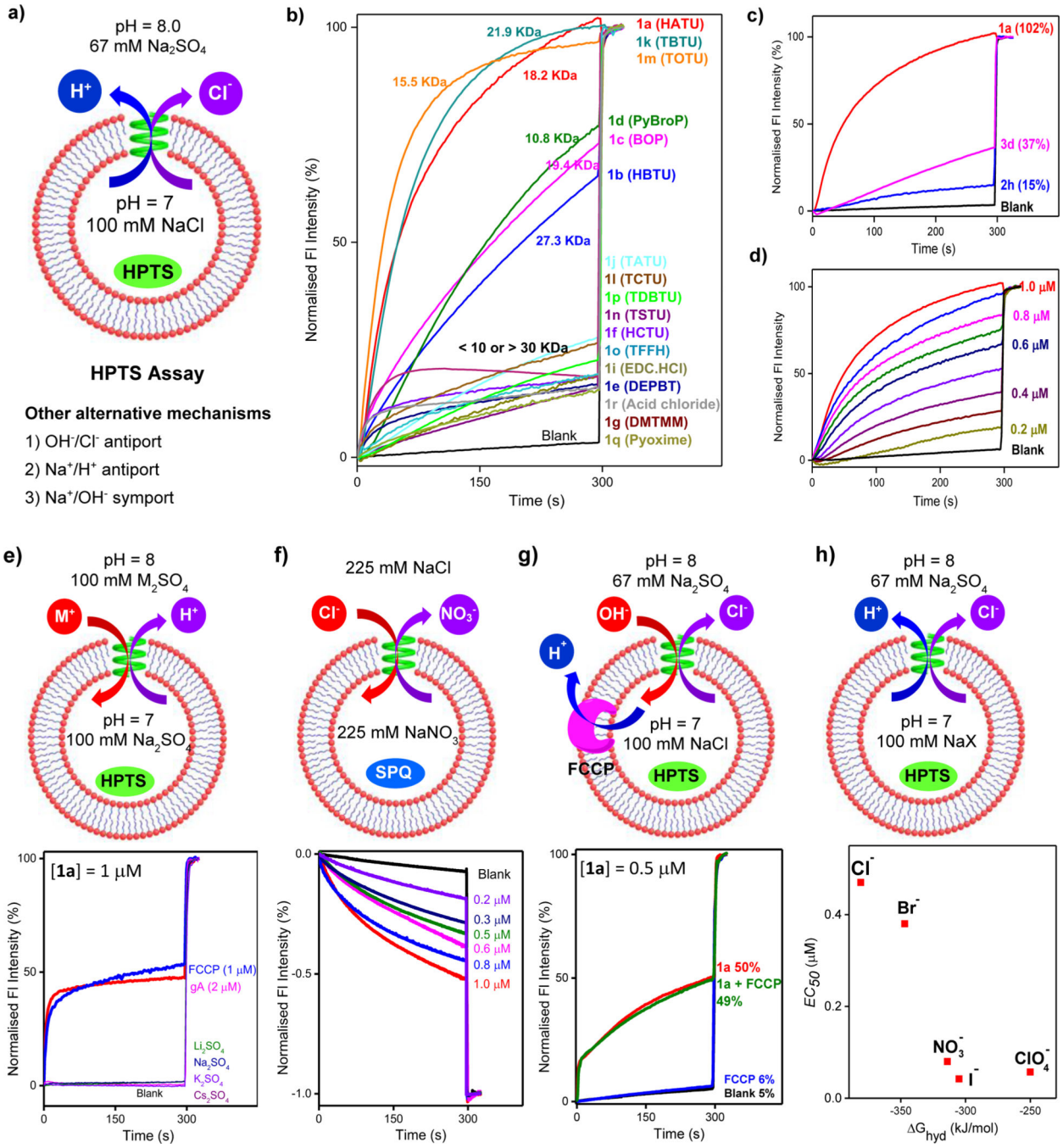


**Figure 2.**

a) Evaluation of ion transport activity of ion channels through a pH-sensitive HPTS assay and possible mechanisms. b) Ion transport activities of **1a–1g** and **1i–1r** at 1 μM. c) Comparison of ion transport activities of the best channels **1a**, **2h** and **3d** from their respective categories **1**, **2**, and **3** at 1 μM. d) Dose-dependent transport activities of **1a**. e) HPTS assay with varied extravesicular cations ($M_2SO_4$) for studying cation selectivity. f) SPQ assay via nitrate/chloride exchange for confirming chloride as the transport species. g) FCCP-coupled HPTS assay for elucidating the role of proton in chloride transport. h) HPTS

assay with varied intravesicular anions (NaX) for studying anion selectivity and determining the corresponding $EC_{50}$ values. In b)-e) and g), fluorescence intensity after addition of Triton X-100 at t = 300 s was set to 100%.

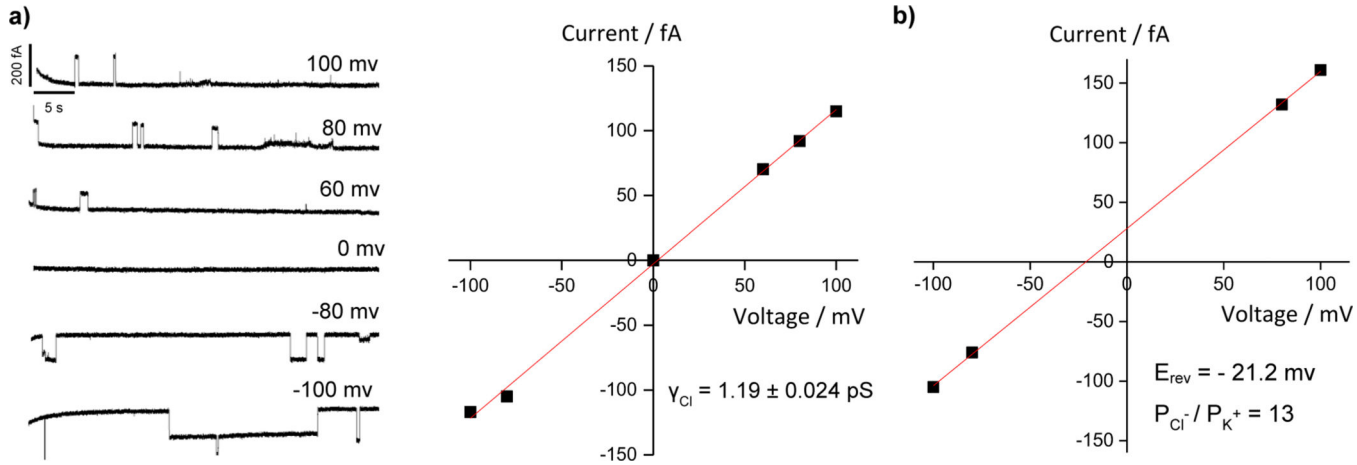


**Figure 3.**

a) Single channel current traces recorded at various voltages recorded in symmetric baths (*cis* chamber = *trans* chamber = 1 M KCl; linear fitting of current–voltage (I-V) plot gives Cl-conductance value (γCl) of 1.19 ± 0.024 pSfor **1a**–mediated transport of chloride. b) Linear fitting of current–voltage (I-V) plot gives Cl-/K+selectivity of 13 for **1a**–mediated transport of chloride; for the corresponding current traces, see FigureS18.

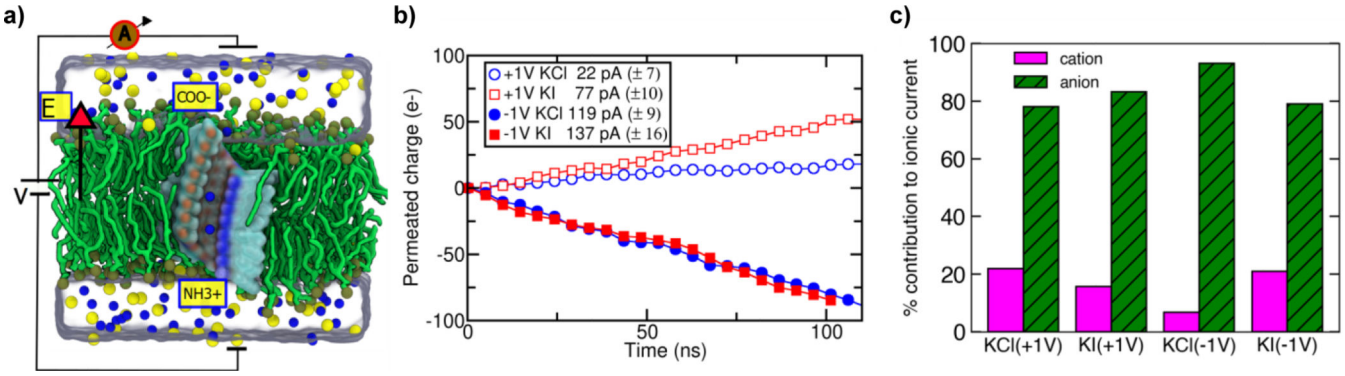


**Figure 4:**

Ionic-current through the **HP24** channel simulated using the all-atom MD method. a) A cut-away view of the simulation system where the channel is shown as a molecular surface coloured according to the local atom types: red (oxygen), blue (nitrogen) and cyan (carbon). The yellow labels specify the location of the terminal groups of the channels. Nitrogen atoms of the lipid head groups are shown as tan sphere whereas the tails of the lipid molecules are shown as thick green lines. $K^+$ (yellow) and $Cl^-$ (blue) ions (at 1 M concentration) are shown as spheres whereas the volume occupied by water is represented by a semi-transparent surface. b) The total permeated charge (integrated ionic current) as a function of the simulation time in the units of the elementary charge, e. The slope of each line gives the average current. The inset specified the average current values with the error bars for each system. c) Percentage of total current carried by the cation and anion species in the simulations of the KCl and Kl systems.

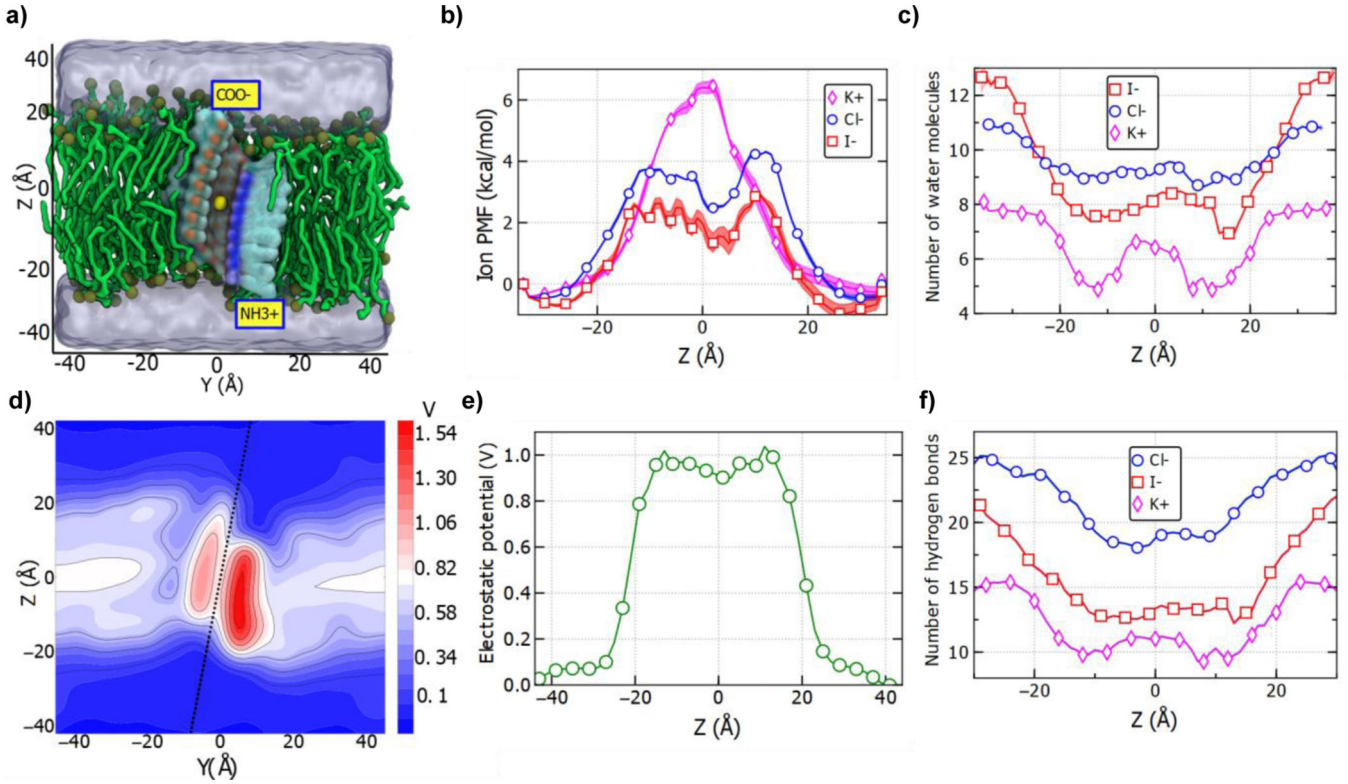


**Figure 5:**

Free-energy and molecular mechanism of ion permeation through an **HP24** channel. a) Cut-away view of the simulation system used for replica-exchange umbrella sampling simulation. In each replica system, a single ion was harmonically restrained to the center of a 1Å wide window; 69 such windows spanned the full range of Z-values in 1 Å interval. b) The free energy of ions permeating across the membrane through the **HP24** channel. The shadowed region shows the standard error in the measurements of PMF. c) The average number of water molecules in the first solvation shell of the permeating ion as a function of its position along the bilayer normal (z-axis). d) An electrostatic potential map of the HP-24 channel in lipid bilayer membrane averaged over 50 ns of equilibrium MD simulation using the PMEpot plugin of VMD; a dotted blue line passing through the center shows the tilted axis of the channel along the bilayer normal. e) The average electrostatic profile along the transmembrane pore of the channel (dotted line in Figure 5d). The potential values were averaged over a 2 Å cylinder coaxial with the axis of the channel. f) The average number of hydrogen bonds formed by the water molecules from the ion's first solvation shell with the rest of the system versus the Z coordinate of the ion.